Structure
Article

Structure of an Asymmetric Ternary Protein Complex Provides Insight for Membrane Interaction

Brian R. Dempsey,[1,3] Atoosa Rezvanpour,[1,3] Ting-Wai Lee,[2,3] Kathryn R. Barber,[1] Murray S. Junop,[2] and Gary S. Shaw[1,*]
[1]Department of Biochemistry, The University of Western Ontario, London, Ontario N6A 5C1, Canada
[2]Department of Biochemistry and Biomedical Sciences, McMaster University, Hamilton, Ontario L8N 3Z5, Canada
[3]These authors contributed equally to this work
*Correspondence: gshaw1@uwo.ca
http://dx.doi.org/10.1016/j.str.2012.08.004

SUMMARY

Plasma membrane repair involves the coordinated effort of proteins and the inner phospholipid surface to mend the rupture and return the cell back to homeostasis. Here, we present the three-dimensional structure of a multiprotein complex that includes S100A10, annexin A2, and AHNAK, which along with dysferlin, functions in muscle and cardiac tissue repair. The 3.5 Å resolution X-ray structure shows that a single region from the AHNAK C terminus is recruited by an S100A10-annexin A2 heterotetramer, forming an asymmetric ternary complex. The AHNAK peptide adopts a coil conformation that arches across the heterotetramer contacting both annexin A2 and S100A10 protomers with tight affinity (~30 nM) and establishing a structural rationale whereby both S100A10 and annexin proteins are needed in AHNAK recruitment. The structure evokes a model whereby AHNAK is targeted to the membrane surface through sandwiching of the binding region between the S100A10/annexin A2 complex and the phospholipid membrane.

INTRODUCTION

The plasma membrane is the physical boundary that separates the intracellular components from the extracellular environment. Although the membrane allows the selective passage of small molecules, its major roles are to maintain homeostasis, to maintain the integrity of internal organelles, and to protect against entry of toxins. Some cells, especially those in muscle tissue are subject to frequent tearing, disrupting the cell membrane. Diseases, such as limb-girdle muscular dystrophy and a variety of myopathies, have been linked to the mutation of proteins involved in membrane repair (Bansal et al., 2003; Illarioshkin et al., 2000; Liu et al., 1998). Dysferlin is one such protein that has been shown to bind with phospholipids in a Ca^{2+}-dependent manner and appears to function by mediating vesicle clustering and fusion with the plasma membrane (Davis et al., 2002) (Cenacchi et al., 2005). The absence of dysferlin in mouse model systems prevents the resealing of plasma membranes (Han et al., 2007; Humphrey et al., 2012). These observations are consistent with one model for membrane repair whereby multiple proteins, including dysferlin, mediate the fusion of an exocytotic compartment to the inner surface of the membrane, thereby expanding and resealing the membrane (Draeger et al., 2011; Han and Campbell, 2007; Idone et al., 2008).

Enlargeosomes are one type of exocytotic vesicle implicated in membrane repair because of their rapid calcium-dependent translocation from the cytosol to the plasma membrane surface immediately following membrane damage (Borgonovo et al., 2002; Cocucci et al., 2004, 2007). Associated with enlargeosomes is AHNAK, a component of the membrane repair complex that interacts with dysferlin (Cacciottolo et al., 2011; de Morrée et al., 2010; Huang et al., 2007, 2008). AHNAK colocalizes with dysferlin at the plasma membrane (Huang et al., 2007), and siRNA knockdown experiments of AHNAK inhibit membrane clustering and fusion (Han et al., 2012). In patients with limb-girdle muscular dystrophy caused by mutation of the dysferlin gene, AHNAK no longer localizes to the plasma membrane in muscle cells (Zacharias et al., 2011).

The enlargeosome and plasma membrane surfaces are also characterized by localization of the calcium-binding protein annexin A2, a protein required for exocytosis, membrane aggregation (Harder and Gerke, 1993, 1994; Illien et al., 2010; Lorusso et al., 2006), and the fusing of two adjacent surfaces (Lennon et al., 2003; McNeil et al., 2006). Annexin A2 has been shown to associate with dysferlin by coimmunoprecipitation, and both proteins colocalize at the plasma membrane (Lennon et al., 2003). Annexin A2 was originally identified as a component of a heterotetrameric complex with S100A10 (also known as p11) (Gerke and Weber, 1985; Glenney and Tack, 1985), a member of the EF-hand S100 family. An S100A10 dimer can coordinate two annexin A2 proteins through a high-affinity interaction with the N terminus of each annexin protein (Becker et al., 1990; Glenney et al., 1986; Johnsson et al., 1988). Upon membrane rupture and calcium influx annexin, A2 localizes to the plasma membrane through phospholipid binding (Swairjo et al., 1995). The ability of the S100A10-annexin A2 complex to bridge adjacent phospholipid membranes during a membrane fusion event has been suggested as an attractive model for membrane repair (Gerke and Moss, 2002). Direct interaction between S100A10, AHNAK, and annexin A2 has been observed in coimmunoprecipitation and yeast three-chimeric experiments, whereas knockdown of either S100A10 or annexin A2 prevents AHNAK from localizing to the membrane (Benaud et al., 2004; De Seranno et al., 2006). Further, proteomic studies have identified AHNAK, annexin A2, and S100A10 as constituent proteins of the dysferlin

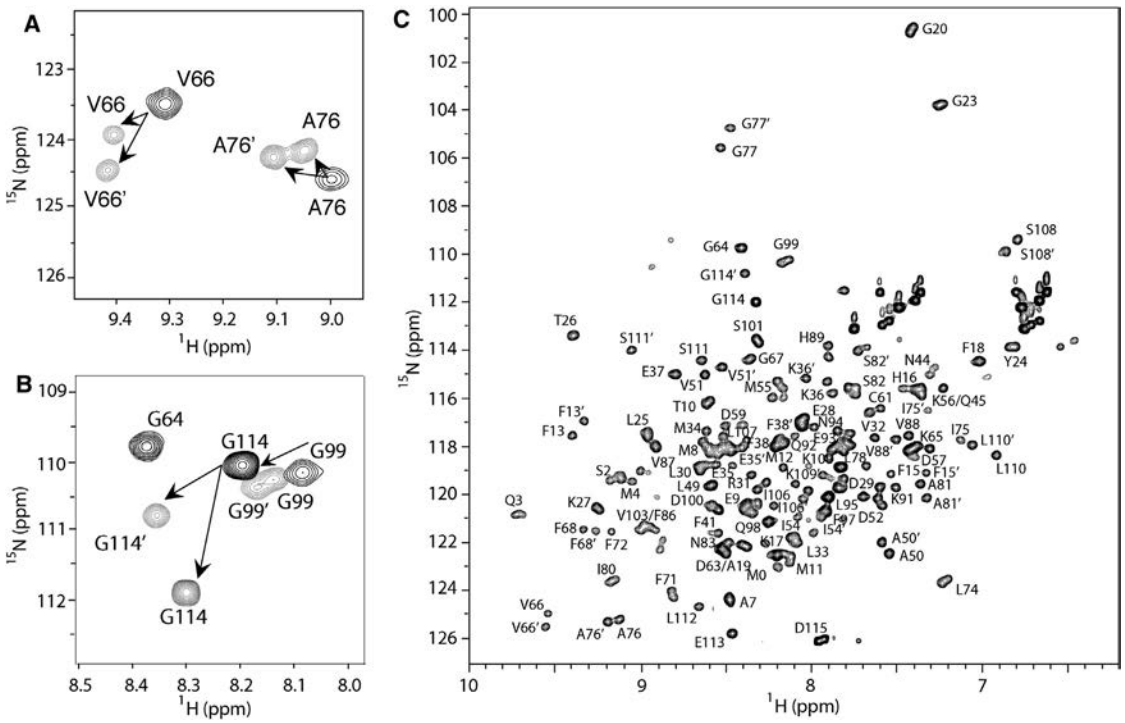

Figure 1. Asymmetry of AHNAK Binding to A10A2 Shown by NMR Spectroscopy

(A and B) Regions of the 600 MHz ^{1}H-^{15}N HSQC spectra for ^{15}N-labeled A10A2 (400 μM) in the absence (dark contours) and presence (light contours) of AHNAK peptide (550 μM).

(C) The assigned ^{1}H-^{15}N HSQC spectrum of A10A2 in complex with the AHNAK peptide. Nonequivalent pairs of residues are indicated by residue and sequence number (i.e., A76, A76'). Residues S101–D115 in A10A2 correspond to residues S1–D15 in annexin A2.

membrane repair complex (Cacciottolo et al., 2011; de Morrée et al., 2010; Leung et al., 2011). Finally, a high-affinity ternary-complex has been identified involving the C terminus of AHNAK with the S100A10-annexin A2 heterotetramer (Rezvanpour et al., 2011).

Membrane repair requires an array of protein-protein interactions near the inner plasma membrane surface and exocytotic vesicles, such as enlargeosomes, to coordinate the resealing process. In this work we describe the 3.5 Å resolution crystal structure of the ternary complex between S100A10, the N terminus of annexin A2 and the binding region from the enlargeosome protein AHNAK. To our knowledge, this is the first structure showing how these three proteins interact prior to association with a membrane required for the repair process.

RESULTS AND DISCUSSION

The assembly of a heterotetrameric complex between S100A10 and annexin A2 has been shown previously to require only the first ten residues from annexin A2 (Becker et al., 1990). To facilitate a stable complex, we constructed a tandem chimeric protein linking the C terminus of S100A10 to the N-terminal 15-residues of annexin A2 separated by a nine-residue tether (A10A2). Comparison of ^{1}H-^{15}N HSQC spectra shows the assembly of this chimeric A10A2 protein is very similar to that of the heterotetrameric noncovalent complex that includes S100A10 and two 14-residue annexin A2 peptides (Rezvanpour et al., 2009). A variety of in vivo and in vitro studies have shown that a small region (G5654–L5673) within the 1,000-residue C terminus of AHNAK interacts with high affinity (~30 nM) with the S100A10-annexin A2 complex or A10A2 (Benaud et al., 2004; De Seranno et al., 2006; Rezvanpour et al., 2011). To identify how S100A10, annexin A2, and AHNAK interact simultaneously the three-dimensional structure was determined of a 20-residue peptide from AHNAK (residues G5654-L5673) in conjunction with the A10A2 chimeric protein.

NMR Experiments Show the Asymmetric Recruitment of AHNAK

The interaction between AHNAK and A10A2 was initially characterized by nuclear magnetic resonance (NMR) spectroscopy. In the absence of the AHNAK peptide the ^{1}H-^{15}N HSQC of A10A2 showed single resonances for residues in both the S100A10 and annexin A2 moieties consistent with the symmetrical nature of the complex (Figure 1). Addition of unlabeled AHNAK peptide (G5654–L5673) to a solution of ^{15}N, ^{13}C-labeled A10A2 resulted in an increased number of peaks, many as pairs, with each signal having about 50% of the original peak intensity (Figure 1). For example, V66 and A76 in the S100A10 moiety, and G99 and G114 in the annexin A2 segment of A10A2, are initially present as single resonances in ^{1}H-^{15}N HSQC spectra but result in two signals upon addition of AHNAK peptide. Assignment of the A10A2-AHNAK complex using triple-resonance experiments indicated that the paired signals arose from identical residues

Table 1. Data Collection and Model Refinement Statistics

Data Collection	
Wavelength (Å)	1.100
Resolution limits[a] (Å)	43.34–3.26 (3.32–3.26)
Space group	P1
Unit-cell constants	
a, *b*, *c* (Å)	47.76, 47.79, 62.82
α, β, γ (°)	71.62, 71.63, 68.62
Number of unique reflections	7,306 (386)
Redundancy	3.8 (3.7)
Completeness (%)	98.6 (100.0)
R_{sym} (%)	8.9 (45.5)
$I / \sigma(I)$	8.9 (3.1)
Wilson B (Å^2)	124.19
Model Refinement	
Resolution range (Å)	43.34–3.50
R_{work} / R_{free} (%)	29.63 / 32.67
Number of nonhydrogen atoms per asymmetric unit (average *B* factors, Å^2)	
Protein	3,496 (154.60)
Solvent	N/A
Rmsd from ideal geometry	
Bond lengths (Å)	0.014
Bond angles (°)	1.165
Ramachandran statistics	
Most favored (%)	73.7
Additional allowed (%)	24.7
Generously allowed (%)	1.3
Disallowed (%)	0.3

[a]Numbers in the parentheses refer to the highest resolution bins.

in S100A10 and annexin A2 that experienced two different environments when in complex with AHNAK (Figure 1). This observation is indicative of an asymmetric binding arrangement for the AHNAK peptide with respect to A10A2. This conclusion is in agreement with previous titration experiments using fluorescence spectroscopy and isothermal calorimetry (Rezvanpour et al., 2011) that show a stoichiometry of one AHNAK peptide per A10A2 tetrameric complex.

Three-Dimensional Structure of A10A2-AHNAK Peptide

Diffraction-quality crystals of the A10A2-AHNAK complex were obtained using the hanging-drop vapor diffusion method. Crystals grew in the space group P1, diffracted to 3.5 Å and contained two copies of the complex linked by disulfide bonds between chains A-C and B-D. Similar disulfide bonding was observed in the structure of S100A10 (Réty et al., 1999). The initial Fo-Fc electron density map following molecular replacement clearly indicated the presence of a single extended peptide within each copy of the A10A2 complex (Figure S1 available online; Table 1). Electron density for the peptide was of sufficient quality to identify residues with bulky hydrophobic side chains. As a result the orientation of the peptide is well defined, despite the medium resolution of the structure. The data allowed fitting of residues P1–K91 in the S100A10 portion of all four chains and S101–L112 (chains A and C) and S101'–E113' (chains B and D) within the annexin A2 portion of A10A2. The nine-residue linker connecting S100A10 to the annexin A2 peptide was dynamically disordered and not modeled in the final structure, suggesting that this region does not associate with either of the protein components in the A10A2 complex. The structure of each complex differed only slightly (backbone rmsd 0.2 Å), and therefore only one complex is described further.

The structure shows a symmetrical arrangement of the S100A10 dimer (Figure 2) with each of the two protomers comprising four α helices (I, Q3–A19; II, K27–K36; III, A50–L58; IV, F68–V88; also I'–IV') that make up the EF-hand motifs, separated by a 12-residue linker containing a short helix (αL, αL'), observed in some other S100 proteins. Helices I and IV (I', IV') comprise the S100A10 dimer interface, forming an X-type bundle originally described for calcium-free S100A6 (Potts et al., 1995). The two N-terminal annexin A2 regions of the A10A2 dimer form α-helical structures (V103 to S108) positioned on opposite sides of the S100A10 protein within a hydrophobic groove formed by helices IV (IV') and αL (αL'). The N terminus (V103, V103') of annexin A2 lays across helix I (I') of the symmetrically related protomer, thereby bridging the S100A10 dimer. The overall structure of the A10A2 chimeric protein within the ternary complex agrees well with the parent complex (Réty et al., 1999) in the absence of AHNAK (backbone rmsd 1.02 Å). This indicates that AHNAK binding to the A10A2 complex does not cause a large structural rearrangement within the heterotetramer.

Consistent with NMR observations, only one AHNAK peptide is present in the A10A2 complex. Although the peptide used in crystallization trials comprised 20 residues, only residues P5659-F5668 were visible in the complex (Figure S1). The AHNAK peptide adopts a coil conformation that arches across helices IV and IV' with its N termini and C termini adjacent to helices III and αL, and III' and αL', respectively, of the S100A10 protein (Figure 2). Both the N termini and C termini of AHNAK are in contact with the C termini of both annexin A2 segments. This places residues at the center of AHNAK (I5663, P5664) near the axis of the helix IV-IV' crossing point (S73, G77, S73', G77'). Moving outward, the N- and C-terminal residues in AHNAK, although different in sequence, have nearly identical contacts with S100A10 and annexin A2 across the interface. This imparts a pseudosymmetric quality to the structure. For example, P5659 packs between residues on helices αL (F41), IV (G77, L78, A81) and annexin A2 (L110, L112) compared with F5668 that has interactions with αL' (F41'), IV' (G77', L78', A81') and annexin A2′ (L110', L112′) on the opposite side of the complex. Similarly, the side chain of M5661 sits among side chains of residues on helices III (I54) and IV (L74, L78), while residue F5666 has contacts with similar residues on the partner protomer. Most of these residues in S100A10 and annexin A2 also experience the largest chemical shift changes and peak duplication upon AHNAK binding observed in NMR experiments (Figure 1). The AHNAK interaction buries about 670 Å^2 of side chain surface area, partitioned among S100A10 (535 Å^2) and annexin A2 (135 Å^2). This shows that both the S100A10 and annexin A2 moieties are required for AHNAK recruitment.

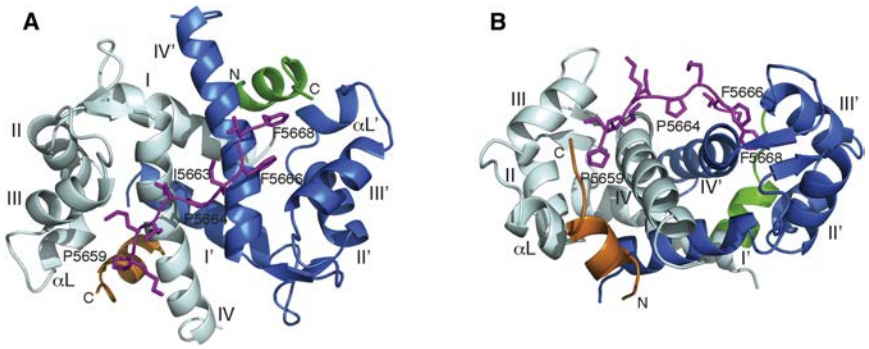

Figure 2. The Structure of the A10A2-AHNAK Ternary Complex

(A) Ribbon diagram of the complex indicating the two S100A10 protomers (blue, cyan), the two annexin peptides (green, orange), and the bound AHNAK peptide (magenta). Only the side chains in the AHNAK peptide are shown for clarity. Residues in AHNAK with key interactions with A10A2 are labeled.

(B) Ribbon diagram from (A) rotated approximately 90° around the x axis showing that AHNAK bends across helices IV and IV' with its N termini and C termini surrounded by helices IV (IV'), III (III'), αL (αL'), and the C termini of both annexin A2 peptides.

See also Figure S1.

The structure of the ternary complex between AHNAK and S100A10-annexin A2 does not resemble any other binding arrangement used by an S100 protein. For example, structures of S100B with peptides derived from p53 (Rustandi et al., 2000) or Ndr kinase (Bhattacharya et al., 2003) utilize a hydrophobic cleft formed by helices III and IV (III', IV') from each protomer, as opposed to AHNAK that crosses helices IV and IV'. Recently, a binary complex between S100A4 and nonmuscle myosin IIA showed the myosin peptide also bound across helices IV and IV' of S100A4 (Elliott et al., 2012; Kiss et al., 2012). Unlike the coil structure adopted by AHNAK, the myosin peptide uses a longer binding sequence and takes on an α-helical structure in the complex. Further, in the A10A2 assemblage with AHNAK both the S100A10 and annexin A2 proteins each make contact with AHNAK, indicating that both proteins are necessary for ternary complex formation. This conclusion corroborates findings that AHNAK displays poor binding with S100A10 alone but displays a dissociation constant near 30 nM in the presence of the N terminus of annexin A2 (De Seranno et al., 2006; Rezvanpour et al., 2011).

Identification of Key Residues at the A10A2 Interface with AHNAK

A peptide array experiment was used to identify residues in AHNAK that are important for formation of the A10A2-AHNAK complex (Figure 3). In two separate experiments, all 20 naturally occurring amino acids were systematically substituted at each position of the AHNAK peptide, synthesized as spots on a nitrocellulose membrane, and probed with fluorescently labeled A10A2. The majority of positions in AHNAK showed little difference in fluorescence intensity compared to the wild-type sequence, indicating these residues were unaffected by substitution. However, several key residues were identified, including I5663, P5664, F5666, and F5668, that reproducibly showed poorer binding for A10A2 based on decreased fluorescence intensity for individual spots. In particular, substitution of either F5666 or F5668 in AHNAK to any residue type other than a large aromatic, resulted in nearly complete loss of A10A2 binding. These two aromatic residues in AHNAK appear as the key anchoring residues for its interaction with A10A2 having multiple hydrophobic contacts with both S100A10 and annexin A2. Residue P5664 was also selective showing poorer binding for most polar residues (K, H, R, E, Q, S, T, A, G). In general these observations agreed with the key hydrophobic residues in AHNAK (P5664, F5666, F5668) located at the interface of the A10A2 structure (Figure 2). One anomaly was P5659 that showed little sensitivity toward substitutions, perhaps indicating that the N-terminal portion of the AHNAK binding sequence makes a smaller contribution to the overall association with S100A10-annexin A2.

Results from the crystal structure and peptide array experiments identified several key residues in S100A10 and annexin A2 at the interface with AHNAK. In particular S73 and S73' appear to act as "guideposts" that funnel the AHNAK peptide across G77 and G77' of helices IV and IV', allowing residues I5663 and P5664 from AHNAK to move into close contact with S100A10 (Figure 4). In addition, the hydroxyl side chains of S73 and S73' are positioned to form hydrogen bonds with the carbonyl oxygens of K5662 and K5665 in AHNAK. To test the importance of S73 and G77 in S100A10 toward AHNAK complex formation these two positions were exchanged (S73G, G77S; A10A2-GS). This should have the effect of changing the angle the AHNAK peptide might adopt upon crossing helices IV and IV', perhaps limiting the ability of the N- and C-terminal regions of AHNAK to contact the C termini of both annexin A2 segments. Rather than restricting experiments to the short 20-residue peptide-binding region, affinity experiments were completed using a 320-residue C-terminal fragment of AHNAK ($AHNAK^{5362–5681}$) and a set of substituted GST-tagged A10A2 proteins. The results showed that wild-type GST-A10A2 bound to $AHNAK^{5362–5681}$ (Figure 4). Upon swapping residues S73 and G77, binding of $AHNAK^{5362–5681}$ to A10A2-GS was reproducibly reduced by about 60%, indicating that the arrangement of these residues is important for maintaining the trajectory of the AHNAK peptide across helices IV and IV'. A further L112A substitution (A10A2-GSA) was made in the annexin A2 region of A10A2. This residue sits adjacent to P5659 (L112) and F5668 (L112′) at the N termini and C termini of AHNAK in the ternary complex (Figure 4) but does not participate in S100A10-annexin A2 complex formation (Becker et al., 1990; Réty et al., 1999), indicating its positioning is unique to the recruitment of AHNAK. When combined with the S73, G77 exchange substitutions, substitution at L112 showed that binding to AHNAK was nearly abolished (>90% reduction).

The three substitutions made in A10A2 indicate that S73 and G77 in S100A10 and L112 in annexin A2 are integral for AHNAK

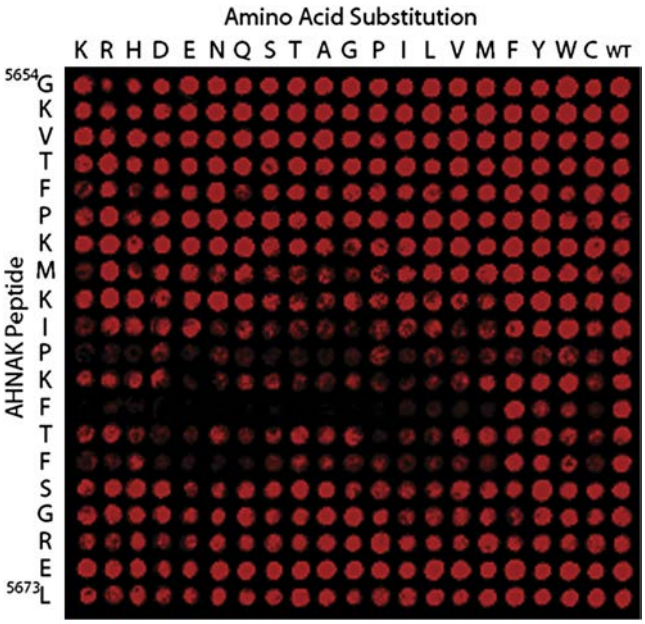

Figure 3. Permutation Peptide Array Showing Key Residues in AHNAK Required for Ternary Complex Formation

AHNAK peptides (20 residues each) were synthesized on a membrane spot array. Substitutions cycle through the naturally occurring amino acids at every position in the AHNAK peptide sequence. The column marked "WT" (far right) contains spots from the wild-type peptide for comparison. The array was probed with 5 nM Alexa-680 labeled A10A2 that fluoresces red.

recruitment and may provide a unique platform for ternary protein assembly. An examination of other S100 protein sequences (Figure S2) shows that only S100A10 possesses the S73/G77 "guideposts" on the surface of helices IV and IV' used to funnel AHNAK across these helices. Typically, the S73 position is occupied by larger residues (V, F) in other S100 proteins and is rarely combined with a glycine residue as observed in S100A10. In addition, the tandem pair of leucine residues (L110, L112) in the N-terminal region of annexin A2 is instrumental in recruiting AHNAK through interactions with F5668. These leucine residues are only found in annexins A2 and A9 (Figure S2), although annexin A9 does not appear to interact with S100A10 based on proteomic analyses of at least one membrane repair complex (de Morrée et al., 2010). Because other molecules, such as the epithelial calcium channel proteins TRPV5 and TRPV6 (Borthwick et al., 2008; van de Graaf et al., 2003) and plasminogen (Kwon et al., 2005; MacLeod et al., 2003), are also recruited by the S100A10-annexin A2 heterotetramer it is likely that a similar ternary binding arrangement exists for these complexes with S100A10-annexin A2.

In complementary reverse affinity experiments, four substitutions in the C terminus of AHNAK$^{5362–5681}$ at positions P5659, I5663, P5664, and F5668 were made and tested for their interaction with GST-A10A2 (Figure 4). Because the structure revealed that AHNAK adopted a coil-type structure, glycine was used for all substitutions to minimize potential backbone disruptions. In the I5663G, P5664G substituted AHNAK protein (AHNAK-IP) a 40% reduction in binding was noted to GST-A10A2 in eluted fractions (Figure 4). A similar result occurred for the P5659G, F5668G (AHNAK-PF) protein. The combination of these four substitutions (AHNAK-PIPF) reproducibly led to a 70% decrease in the amount of AHNAK protein bound to GST-A10A2. These observations correspond to approximate increases in the dissociation constants of 5-fold (AHNAK-IP, AHNAK-PF) and 20-fold (AHNAK-PIPF) compared to the wild-type interaction (30 nM) (De Seranno et al., 2006; Rezvanpour et al., 2011). These results support the importance of I5663 and P5664 residues at the fulcrum of the helix IV-IV' crossing point in S100A10 (Figure 4), nestled between the guidepost residues S73 (S73') and G77 (G77'). The P5659 and F5668 residues in AHNAK are equidistant from the center of the AHNAK sequence and show pseudosymmetric contacts with F41, I54, L78, A81 (F41', I54', L78', A81') from S100A10 and L110 and L112 (L110′, L112′) from annexin A2 (Figures 4D and 4E). Based on the structure, substitution of these four residues (P5659, I5663, P5664, and F5668) would eliminate most hydrophobic contacts and binding between AHNAK and A10A2.

Model of AHNAK Recruitment for Membrane Repair

The structure of the A10A2 ternary complex with the AHNAK peptide provides an attractive model for their roles in membrane repair. Although AHNAK and annexin A2 have been observed to undergo a calcium-mediated translocation to the membrane surface (Benaud et al., 2004; Borgonovo et al., 2002; Cocucci et al., 2004, 2007; Lorusso et al., 2006), neither protein has a membrane spanning sequence. Further, knockdown of either S100A10 or annexin A2 proteins prevents AHNAK from moving to the phospholipid membrane surface. These observations indicate a dependency for AHNAK translocation on calcium influx and on its association with the S100A10-annexin A2 complex. One possible mechanism to account for this could involve calcium binding to the seven calcium-binding sites on the surface of annexin A2. This has been proposed to release the N terminus of the protein allowing interaction with S100A10 (Rosengarth and Luecke, 2003). Further, calcium binding to annexin A2 is a requirement for its association with the inner surface of the phospholipid membrane. These requirements indicate the S100A10-annexin A2 heterotetramer must initially be formed to allow sequential recruitment of AHNAK, moving it to the phospholipid surface as observed in previous experiments (Borgonovo et al., 2002; Cocucci et al., 2004, 2007). The orientation of the N-terminal annexin A2 region in the A10A2-AHNAK complex is such that the calcium-binding portions of annexin A2 lie on the on same face as the C-terminal binding region for AHNAK (Figure 5). It is also possible that a second, lower affinity-binding site located near the N terminus of AHNAK (G302-E321) might also be recruited by the S100A10-annexin A2 complex (De Seranno et al., 2006). The sequence of this N-terminal AHNAK motif includes analogous interfacial residues (P307, M309, V311, P312, F314, V316) to those utilized by the C-terminal fragment studied here for A10A2 interaction. This similarity suggests the N-terminal AHNAK binding motif would likely adopt a similar bound conformation as the C-terminal peptide. In either case, this could cause this portion of AHNAK to be sandwiched between the phospholipid membrane, coordinated to calcium-loaded annexin A2, and S100A10. Because AHNAK is a very large protein (>5,000 residues) the small binding region recruited by S100A10-annexin A2 would allow the

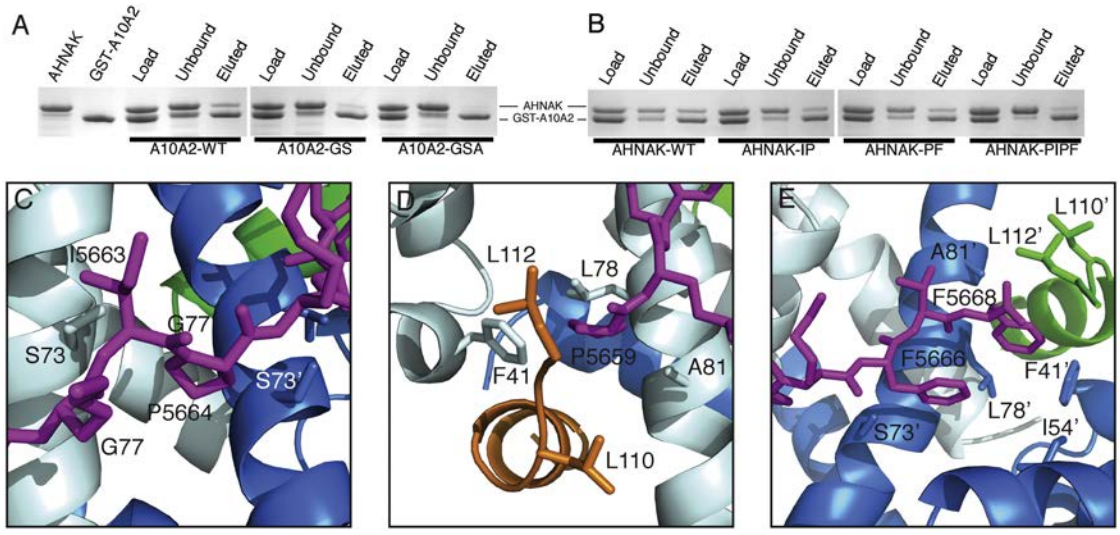

Figure 4. Affinity Experiments Showing the Interaction between a C-Terminal Fragment of AHNAK (AHNAK$^{5362–5681}$) with GST-A10A2

(A) AHNAK$^{5362–5681}$ along with wild-type GST-A10A2 (lanes 3–5), GST-A10A2 having residues S73 and G77 swapped (A10A2-GS, lanes 6–8) or residues S73 and G77 swapped in combination with an L112A substitution in annexin A2 (A10A2-GSA, lanes 9–11) were loaded onto glutathione Sepharose beads.

(B) GST-A10A2 was loaded onto glutathione Sepharose beads along with wild-type AHNAK peptide (AHNAK-WT, lanes 1–3), AHNAK having I5663G and P5664G substitutions (AHNAK-IP, lanes 4–6), AHNAK having P5659G and F5668G substitutions (AHNAK-PF, lanes 7–9), or AHNAK having P5659G, I5663G, P5664G, and F5668G substitutions (AHNAK-PIPF, lanes 10–12). Each series of experiments shows the total protein loaded, unbound protein obtained in the supernatant, and bound protein upon elution with glutathione.

(C–E) Highlighted residues in A10A2 and AHNAK involved in the interactions.

See also Figure S2.

remainder of the AHNAK protein to participate in additional protein interactions, including those with dysferlin. This model is consistent with the proposed scaffolding role for AHNAK to recruit multiple repair molecules to the surface of the phospholipid membrane.

EXPERIMENTAL PROCEDURES

Protein Expression and Purification

The expression/purification of the S100A10-annexin A2 chimeric protein (A10A2) has been previously described (Rezvanpour et al., 2009). Briefly, the A10A2 protein contains residues 1–92 from rabbit S100A10 (100% amino acid sequence identity with the human protein), a nine-residue linker (93–100 that contains a tobacco-etch mosaic virus (TEV) cleavage site followed by the N-terminal 15 residues (101–115) from annexin A2. Unlabeled and uniformly ^{15}N, ^{13}C-labeled GST-tagged human A10A2 were overexpressed and purified in the BL21 (DE3)-RIL *Escherichia coli* strain. For affinity experiments, the GST purification tag was not cleaved from the A10A2 protein. A10A2 proteins all contained the C82S substitution for continuity with previous work (Rezvanpour et al., 2011). The substitutions L112A (A10A2-A), S73G, G77S (A10A2-GS), and S73G,G77S,L112A (A10A2-GSA) were produced using the QuikChange protocol (Stratagene, La Jolla, CA, USA).

A gene construct encoding residues 5362–5681 of human AHNAK was synthesized by DNA2.0 (Menlo Park, CA, USA) and placed in a pJexpress411 vector with a TEV protease cleavage site between the AHNAK protein and an N-terminal 6x-His tag. Substitution mutations P5659G, F5668G (AHNAK-PF), I5663G, P5664G (AHNAK-IP), and P5659G, I5663G, P5664G, F5668G (AHNAK-PIPF) were created using the QuikChange protocol (Stratagene, La Jolla, CA). AHNAK proteins were expressed using *E. coli* BL21(DE3) cells grown in Luria-Bertani (LB) media. At OD_{600} = 0.6 protein expression was induced with 1mM IPTG for 4 hr at 37°C. Cells were resuspended in buffer (50 mM $NaHPO_4$, 500 mM NaCl, and 25 mM Imidazole [pH 7.4]) and lysed by emulsification (Avestin, Ottawa, ON, Canada). The lysate was clarified by ultracentrifugation and then applied to Ni-NTA agarose (Qiagen, Mississauga, ON, Canada). The agarose was washed extensively, and then bound protein was eluted using buffer supplemented with 250 mM Imidazole. Masses of all proteins were confirmed by ESI-MS (UWO Biological Mass Spectrometry Laboratory). The AHNAK peptide (GKVTFPKMKIPKFTFSGREL) was synthesized with N-terminal acetylation and C-terminal amidation (Bio Basic Inc., Toronto, Canada).

NMR Spectroscopy

NMR experiments were collected on a Varian INOVA 600 MHz spectrometer using a pulsed-field gradient triple-resonance probe at 35°C. Samples of uniformly ^{15}N, ^{13}C-labeled A10A2 (400 μM) or selectively labeled ^{15}N-labeled A10A2 proteins (40–110 μM) were prepared in 20 mM MOPS, 1 mM EDTA, 1 mM DTT, 50 mM arginine, 50 mM glutamic acid, 100 mM NaCl, and 90% H_2O/10% D_2O at pH 7.0. AHNAK peptide was added at approximately 10% excess compared to the A10A2 dimer concentration to ensure saturation. ^{1}H-^{15}N HSQC spectra were collected using the sensitivity-enhanced method (Kay et al., 1992). Backbone resonance assignments for the A10A2-AHNAK peptide complex were completed using standard triple-resonance methods (Grzesiek and Bax, 1992; Kay et al., 1990; Wittekind and Mueller, 1993). All data were processed and analyzed using NMRPipe/NMRDraw (Delaglio et al., 1995) and NMRView (Johnson and Belvins, 1994).

Crystallization and Structure Determination

The A10A2-AHNAK peptide complex was purified using a HiPrep 26/10 desalting column (GE Healthcare, Uppsala, Sweden) equilibrated in 50 mM Tris-HCl and 1 mM DTT at pH 7.5. Crystals of the complex were obtained using the hanging-drop vapor diffusion method using the A10A2-AHNAK complex (8 mg/ml) mixed with an equal volume (1 μl) of precipitant (Qiagen Nucleix Suite #85: 100 mM NaCl, 200 mM $MgCl_2$, and 0.05 M $(CH_3)_2AsO_2Na$, 20% [w/v] PEG-1000 [pH 6.5]), and crystallization additive (Hampton Research Additive Screen #68: 0.15 mM CYMAL-7, 0.2 μl). The reservoir contained 1.5 M $(NH_4)_2SO_4$ (500 μl). Diffraction-quality crystals (200 × 200 × 100 μm^3) grew in about five days at 20°C and were flash-cooled in liquid nitrogen prior to data collection. X-ray diffraction data were collected at Beamline X25

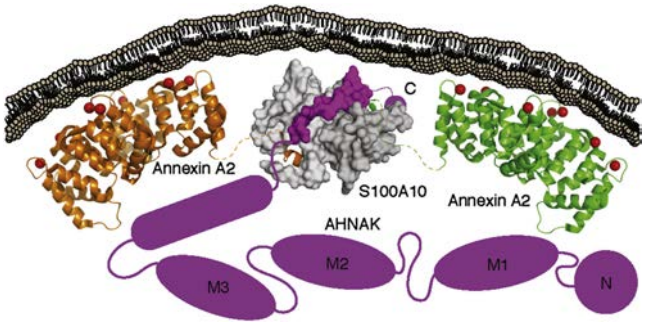

Figure 5. Model of AHNAK Recruitment to the Phospholipid Membrane by the S100A10-Annexin A2 Complex

The model shows S100A10 (gray) in complex with the N-terminal region of annexin A2 (orange, green) and the C-terminal binding region from AHNAK (space filled, magenta, residues 5654–5673). The calcium-binding core region of annexin A2 is shown in its calcium-bound state (2HYW), the active state for its association with a phospholipid membrane (top). The N-terminal region of annexin A2 bound to S100A10 shown in the structure is separated by only 15 residues from the core region, indicating the two proteins must be in close proximity. The 700 kDa protein AHNAK (magenta) is depicted schematically to show its 250-residue N-terminal domain (N), three central 500-residue repeat sections (M1, M2, and M3), and 1,000 residue C terminus that includes the S100A10-annexin A2 binding sequence. Based on the model, derived from the A10A2 structure in complex with the AHNAK peptide, the S100A10 and annexin A2 proteins would sandwich the AHNAK binding region near the phospholipid membrane, leaving the remainder of AHNAK to employ its scaffolding role.

(equipped with an ADSC Q315 CCD detector) at the National Synchrotron Light Source in Brookhaven National Laboratory. X-ray diffraction data was indexed, scaled, and merged using HKL-2000 (Otwinowski and Minor, 1997). Initial phases were obtained by molecular replacement, using the structure of p11 bound to an annexin A2 N-terminal peptide as search model (PDB ID code 1BT6) (Réty et al., 1999). Molecular replacement and model refinement were performed using PHENIX (Adams et al., 2010) and CNS (Brünger et al., 1998), respectively. During refinement, the structural model was adjusted manually when needed using Coot (Emsley et al., 2010). The stereochemical quality of the structural model was assessed using PROCHECK (Laskowski et al., 1993). Structural comparison (backbone rmsd) calculations and graphical representations of the structural model were prepared using PyMOL (Version 1.2r2, Schrödinger, LLC). The interactions between A10A2 and the AHNAK peptide were analyzed using the program VADAR (Volume, Area, Dihedral Angle Reporter) (Willard et al., 2003).

Protein Affinity Experiments

For GST-based affinity experiments, all proteins were dialyzed into three changes of PBS buffer (10 mM Na_2HPO_4, 1.8 mM KH_2PO_4, 140 mM NaCl, and 2.7 mM KCl [pH 7.3]) supplemented with 0.5 mM EDTA and 0.5 mM TCEP. GST-A10A2 and AHNAK proteins (5 μM each) were mixed and incubated for 20 min at 20°C. Protein mixtures were added to loose glutathione Sepharose 4B beads (80 μl) (GE Healthcare) equilibrated in PBS buffer and incubated at 20°C for an additional 20 min with gentle rocking. Beads were washed three times with PBS buffer (500 μl) and bound protein eluted with a 50 mM Tris, 20 mM glutathione solution at pH 8.0 (160 μl). Samples of the applied protein mixture, unbound and eluted proteins were separated on 10% Tris-Tricine gels and assessed by densitometry.

Peptide Array Experiments

Permutation peptide array experiments used a series of 20-residue AHNAK peptides (residues 5654–5673). Each peptide was synthesized on a nitrocellulose membrane using an Auto-Spot robot ASP222 (Amimed, London, UK) using F-moc chemistry. Every position in the AHNAK peptide was systematically substituted with each of the 20 naturally occurring amino acids. The resulting spot array was 20×20 with an additional control column representing the wild-type AHNAK peptide. A10A2-C82S protein was fluorescently labeled with AlexaFluor 680 maleimide, as described previously, (Invitrogen, Eugene, OR, USA) on Cys62 (Rezvanpour et al., 2011). The membrane was probed with 5 nM A10A2 in TBS buffer (20 mM Tris and 150 mM NaCl [pH 7.0]) supplemented with 0.05% Tween-20 and 3% BSA for 2 hr and then rinsed with TBS buffer supplemented with 0.05% Tween-20. Arrays were imaged using an Odyssey imaging instrument (LI-COR Biosciences, Lincoln, NE, USA) at 700 nm.

ACCESSION NUMBERS

The Protein Data Bank (http://www.pdb.org) accession number for the structure of the A10A2-AHNAK peptide complex reported in this paper is 4DRW.

SUPPLEMENTAL INFORMATION

Supplemental Information includes two figures and can be found with this article online at http://dx.doi.org/10.1016/j.str.2012.08.004.

ACKNOWLEDGMENTS

This research was supported by the Canadian Institutes of Health Research (MOP-93520 to G.S.S. and MOP-89903 to M.S.J.), a postdoctoral fellowship from the Ontario Ministry of Research and Innovation (to T.W.L.), and the Canada Research Chairs Program (to G.S.S.). Data for this study were measured at beamline X25 of the National Synchrotron Light Source. Financial support comes principally from the Offices of Biological and Environmental Research and of Basic Energy Sciences of the U.S. Department of Energy and from the National Center for Research Resources (P41RR012408) and the National Institute of General Medical Sciences (P41GM103473) of the National Institutes of Health. We thank the National Synchrotron Light Source, Brookhaven National Laboratory, for providing beamline access and Annie Heroux and the beamline staff at X25 for helpful assistance during data collection.

Received: June 7, 2012
Revised: July 31, 2012
Accepted: August 5, 2012
Published online: August 30, 2012

REFERENCES

Adams, P.D., Afonine, P.V., Bunkóczi, G., Chen, V.B., Davis, I.W., Echols, N., Headd, J.J., Hung, L.W., Kapral, G.J., Grosse-Kunstleve, R.W., et al. (2010). PHENIX: a comprehensive Python-based system for macromolecular structure solution. Acta Crystallogr. D Biol. Crystallogr. *66*, 213–221.

Bansal, D., Miyake, K., Vogel, S.S., Groh, S., Chen, C.C., Williamson, R., McNeil, P.L., and Campbell, K.P. (2003). Defective membrane repair in dysferlin-deficient muscular dystrophy. Nature *423*, 168–172.

Becker, T., Weber, K., and Johnsson, N. (1990). Protein-protein recognition via short amphiphilic helices; a mutational analysis of the binding site of annexin II for p11. EMBO J. *9*, 4207–4213.

Benaud, C., Gentil, B.J., Assard, N., Court, M., Garin, J., Delphin, C., and Baudier, J. (2004). AHNAK interaction with the annexin 2/S100A10 complex regulates cell membrane cytoarchitecture. J. Cell Biol. *164*, 133–144.

Bhattacharya, S., Large, E., Heizmann, C.W., Hemmings, B., and Chazin, W.J. (2003). Structure of the Ca2+/S100B/NDR kinase peptide complex: insights into S100 target specificity and activation of the kinase. Biochemistry *42*, 14416–14426.

Borgonovo, B., Cocucci, E., Racchetti, G., Podini, P., Bachi, A., and Meldolesi, J. (2002). Regulated exocytosis: a novel, widely expressed system. Nat. Cell Biol. *4*, 955–962.

Borthwick, L.A., Neal, A., Hobson, L., Gerke, V., Robson, L., and Muimo, R. (2008). The annexin 2-S100A10 complex and its association with TRPV6 is

regulated by cAMP/PKA/CnA in airway and gut epithelia. Cell Calcium *44*, 147–157.

Brünger, A.T., Adams, P.D., Clore, G.M., DeLano, W.L., Gros, P., Grosse-Kunstleve, R.W., Jiang, J.S., Kuszewski, J., Nilges, M., Pannu, N.S., et al. (1998). Crystallography & NMR system: A new software suite for macromolecular structure determination. Acta Crystallogr. D Biol. Crystallogr. *54*, 905–921.

Cacciottolo, M., Belcastro, V., Laval, S., Bushby, K., di Bernardo, D., and Nigro, V. (2011). Reverse engineering gene network identifies new dysferlin-interacting proteins. J. Biol. Chem. *286*, 5404–5413.

Cenacchi, G., Fanin, M., De Giorgi, L.B., and Angelini, C. (2005). Ultrastructural changes in dysferlinopathy support defective membrane repair mechanism. J. Clin. Pathol. *58*, 190–195.

Cocucci, E., Racchetti, G., Podini, P., Rupnik, M., and Meldolesi, J. (2004). Enlargeosome, an exocytic vesicle resistant to nonionic detergents, undergoes endocytosis via a nonacidic route. Mol. Biol. Cell *15*, 5356–5368.

Cocucci, E., Racchetti, G., Podini, P., and Meldolesi, J. (2007). Enlargeosome traffic: exocytosis triggered by various signals is followed by endocytosis, membrane shedding or both. Traffic *8*, 742–757.

Davis, D.B., Doherty, K.R., Delmonte, A.J., and McNally, E.M. (2002). Calcium-sensitive phospholipid binding properties of normal and mutant ferlin C2 domains. J. Biol. Chem. *277*, 22883–22888.

de Morrée, A., Hensbergen, P.J., van Haagen, H.H., Dragan, I., Deelder, A.M., 't Hoen, P.A., Frants, R.R., and van der Maarel, S.M. (2010). Proteomic analysis of the dysferlin protein complex unveils its importance for sarcolemmal maintenance and integrity. PLoS One *5*, e13854.

De Seranno, S., Benaud, C., Assard, N., Khediri, S., Gerke, V., Baudier, J., and Delphin, C. (2006). Identification of an AHNAK binding motif specific for the Annexin2/S100A10 tetramer. J. Biol. Chem. *281*, 35030–35038.

Delaglio, F., Grzesiek, S., Vuister, G.W., Zhu, G., Pfeifer, J., and Bax, A. (1995). NMRPipe: a multidimensional spectral processing system based on UNIX pipes. J. Biomol. NMR *6*, 277–293.

Draeger, A., Monastyrskaya, K., and Babiychuk, E.B. (2011). Plasma membrane repair and cellular damage control: the annexin survival kit. Biochem. Pharmacol. *81*, 703–712.

Elliott, P.R., Irvine, A.F., Jung, H.S., Tozawa, K., Pastok, M.W., Picone, R., Badyal, S.K., Basran, J., Rudland, P.S., Barraclough, R., et al. (2012). Asymmetric mode of Ca^{2+}-S100A4 interaction with nonmuscle myosin IIA generates nanomolar affinity required for filament remodeling. Structure *20*, 654–666.

Emsley, P., Lohkamp, B., Scott, W.G., and Cowtan, K. (2010). Features and development of Coot. Acta Crystallogr. D Biol. Crystallogr. *66*, 486–501.

Gerke, V., and Weber, K. (1985). The regulatory chain in the p36-kd substrate complex of viral tyrosine-specific protein kinases is related in sequence to the S-100 protein of glial cells. EMBO J. *4*, 2917–2920.

Gerke, V., and Moss, S.E. (2002). Annexins: from structure to function. Physiol. Rev. *82*, 331–371.

Glenney, J.R., Jr., and Tack, B.F. (1985). Amino-terminal sequence of p36 and associated p10: identification of the site of tyrosine phosphorylation and homology with S-100. Proc. Natl. Acad. Sci. USA *82*, 7884–7888.

Glenney, J.R., Jr., Boudreau, M., Galyean, R., Hunter, T., and Tack, B. (1986). Association of the S-100-related calpactin I light chain with the NH2-terminal tail of the 36-kDa heavy chain. J. Biol. Chem. *261*, 10485–10488.

Grzesiek, S., and Bax, A. (1992). An efficient experiment for sequential backbone assignment of medium-sized isotopically enriched proteins. J. Magn. Reson. *99*, 201–207.

Han, R., and Campbell, K.P. (2007). Dysferlin and muscle membrane repair. Curr. Opin. Cell Biol. *19*, 409–416.

Han, R., Bansal, D., Miyake, K., Muniz, V.P., Weiss, R.M., McNeil, P.L., and Campbell, K.P. (2007). Dysferlin-mediated membrane repair protects the heart from stress-induced left ventricular injury. J. Clin. Invest. *117*, 1805–1813.

Han, W.Q., Xia, M., Xu, M., Boini, K.M., Ritter, J.K., Li, N.J., and Li, P.L. (2012). Lysosome fusion to the cell membrane is mediated by the dysferlin C2A domain in coronary arterial endothelial cells. J. Cell Sci. *125*, 1225–1234.

Harder, T., and Gerke, V. (1993). The subcellular distribution of early endosomes is affected by the annexin II2p11(2) complex. J. Cell Biol. *123*, 1119–1132.

Harder, T., and Gerke, V. (1994). The annexin II2p11(2) complex is the major protein component of the triton X-100-insoluble low-density fraction prepared from MDCK cells in the presence of Ca2+. Biochim. Biophys. Acta *1223*, 375–382.

Huang, Y., Laval, S.H., van Remoortere, A., Baudier, J., Benaud, C., Anderson, L.V., Straub, V., Deelder, A., Frants, R.R., den Dunnen, J.T., et al. (2007). AHNAK, a novel component of the dysferlin protein complex, redistributes to the cytoplasm with dysferlin during skeletal muscle regeneration. FASEB J. *21*, 732–742.

Huang, Y., de Morrée, A., van Remoortere, A., Bushby, K., Frants, R.R., Dunnen, J.T., and van der Maarel, S.M. (2008). Calpain 3 is a modulator of the dysferlin protein complex in skeletal muscle. Hum. Mol. Genet. *17*, 1855–1866.

Humphrey, G.W., Mekhedov, E., Blank, P.S., de Morree, A., Pekkurnaz, G., Nagaraju, K., and Zimmerberg, J. (2012). GREG cells, a dysferlin-deficient myogenic mouse cell line. Exp. Cell Res. *318*, 127–135.

Idone, V., Tam, C., and Andrews, N.W. (2008). Two-way traffic on the road to plasma membrane repair. Trends Cell Biol. *18*, 552–559.

Illarioshkin, S.N., Ivanova-Smolenskaya, I.A., Greenberg, C.R., Nylen, E., Sukhorukov, V.S., Poleshchuk, V.V., Markova, E.D., and Wrogemann, K. (2000). Identical dysferlin mutation in limb-girdle muscular dystrophy type 2B and distal myopathy. Neurology *55*, 1931–1933.

Illien, F., Finet, S., Lambert, O., and Ayala-Sanmartin, J. (2010). Different molecular arrangements of the tetrameric annexin 2 modulate the size and dynamics of membrane aggregation. Biochim. Biophys. Acta *1798*, 1790–1796.

Johnson, B.A., and Belvins, R.A. (1994). NMRView: a computer program for the visualization and analysis of NMR data. J. Biomol. NMR *4*, 603–614.

Johnsson, N., Marriott, G., and Weber, K. (1988). p36, the major cytoplasmic substrate of src tyrosine protein kinase, binds to its p11 regulatory subunit via a short amino-terminal amphiphatic helix. EMBO J. *7*, 2435–2442.

Kay, L.E., Ikura, M., Tschudin, R., and Bax, A. (1990). Three-dimensional triple-resonance NMR spectroscopy of isotopically enriched proteins. J. Magn. Reson. *89*, 496–514.

Kay, L.E., Keifer, P., and Saarinen, T. (1992). Pure absorption gradient enhanced heteronuclear single quantum correlation spectroscopy with improved sensitivity. J. Am. Chem. Soc. *114*, 10663–10665.

Kiss, B., Duelli, A., Radnai, L., Kékesi, K.A., Katona, G., and Nyitray, L. (2012). Crystal structure of the S100A4-nonmuscle myosin IIA tail fragment complex reveals an asymmetric target binding mechanism. Proc. Natl. Acad. Sci. USA *109*, 6048–6053.

Kwon, M., MacLeod, T.J., Zhang, Y., and Waisman, D.M. (2005). S100A10, annexin A2, and annexin a2 heterotetramer as candidate plasminogen receptors. Front. Biosci. *10*, 300–325.

Laskowski, R.A., Moss, D.S., and Thornton, J.M. (1993). Main-chain bond lengths and bond angles in protein structures. J. Mol. Biol. *231*, 1049–1067.

Lennon, N.J., Kho, A., Bacskai, B.J., Perlmutter, S.L., Hyman, B.T., and Brown, R.H., Jr. (2003). Dysferlin interacts with annexins A1 and A2 and mediates sarcolemmal wound-healing. J. Biol. Chem. *278*, 50466–50473.

Leung, C., Utokaparch, S., Sharma, A., Yu, C., Abraham, T., Borchers, C., and Bernatchez, P. (2011). Proteomic identification of dysferlin-interacting protein complexes in human vascular endothelium. Biochem. Biophys. Res. Commun. *415*, 263–269.

Liu, J., Aoki, M., Illa, I., Wu, C., Fardeau, M., Angelini, C., Serrano, C., Urtizberea, J.A., Hentati, F., Hamida, M.B., et al. (1998). Dysferlin, a novel skeletal muscle gene, is mutated in Miyoshi myopathy and limb girdle muscular dystrophy. Nat. Genet. *20*, 31–36.

Lorusso, A., Covino, C., Priori, G., Bachi, A., Meldolesi, J., and Chieregatti, E. (2006). Annexin2 coating the surface of enlargeosomes is needed for their regulated exocytosis. EMBO J. *25*, 5443–5456.

MacLeod, T.J., Kwon, M., Filipenko, N.R., and Waisman, D.M. (2003). Phospholipid-associated annexin A2-S100A10 heterotetramer and its subunits: characterization of the interaction with tissue plasminogen activator, plasminogen, and plasmin. J. Biol. Chem. *278*, 25577–25584.

McNeil, A.K., Rescher, U., Gerke, V., and McNeil, P.L. (2006). Requirement for annexin A1 in plasma membrane repair. J. Biol. Chem. *281*, 35202–35207.

Otwinowski, Z., and Minor, W. (1997). Processing of X-ray diffraction data collected in oscillation mode. In Methods in Enzymology, C.W. Carter and R.M. Sweets, eds. (Charlottesville: University of Virginia), pp. 307–326.

Potts, B.C.M., Smith, J., Akke, M., Macke, T.J., Okazaki, K., Hidaka, H., Case, D.A., and Chazin, W.J. (1995). The structure of calcyclin reveals a novel homodimeric fold for S100 $Ca^{(2+)}$-binding proteins. Nat. Struct. Biol. *2*, 790–796.

Réty, S., Sopkova, J., Renouard, M., Osterloh, D., Gerke, V., Tabaries, S., Russo-Marie, F., and Lewit-Bentley, A. (1999). The crystal structure of a complex of p11 with the annexin II N-terminal peptide. Nat. Struct. Biol. *6*, 89–95.

Rezvanpour, A., Phillips, J.M., and Shaw, G.S. (2009). Design of high-affinity S100-target hybrid proteins. Protein Sci. *18*, 2528–2536.

Rezvanpour, A., Santamaria-Kisiel, L., and Shaw, G.S. (2011). The S100A10-annexin A2 complex provides a novel asymmetric platform for membrane repair. J. Biol. Chem. *286*, 40174–40183.

Rosengarth, A., and Luecke, H. (2003). A calcium-driven conformational switch of the N-terminal and core domains of annexin A1. J. Mol. Biol. *326*, 1317–1325.

Rustandi, R.R., Baldisseri, D.M., and Weber, D.J. (2000). Structure of the negative regulatory domain of p53 bound to S100B(betabeta). Nat. Struct. Biol. *7*, 570–574.

Swairjo, M.A., Concha, N.O., Kaetzel, M.A., Dedman, J.R., and Seaton, B.A. (1995). Ca(2+)-bridging mechanism and phospholipid head group recognition in the membrane-binding protein annexin V. Nat. Struct. Biol. *2*, 968–974.

van de Graaf, S.F., Hoenderop, J.G., Gkika, D., Lamers, D., Prenen, J., Rescher, U., Gerke, V., Staub, O., Nilius, B., and Bindels, R.J. (2003). Functional expression of the epithelial Ca(2+) channels (TRPV5 and TRPV6) requires association of the S100A10-annexin 2 complex. EMBO J. *22*, 1478–1487.

Willard, L., Ranjan, A., Zhang, H., Monzavi, H., Boyko, R.F., Sykes, B.D., and Wishart, D.S. (2003). VADAR: a web server for quantitative evaluation of protein structure quality. Nucleic Acids Res. *31*, 3316–3319.

Wittekind, M., and Mueller, L. (1993). HNCACB, a high sensitivity 3D NMR experiment to correlate amide-proton and nitrogen resonances with the alpha-carbon and beta-carbon resonances in proteins. J. Magn. Reson., Ser. B. *101*, 201–205.

Zacharias, U., Purfürst, B., Schöwel, V., Morano, I., Spuler, S., and Haase, H. (2011). Ahnak1 abnormally localizes in muscular dystrophies and contributes to muscle vesicle release. J. Muscle Res. Cell Motil. *32*, 271–280.